An EGO-like Optimization Framework for Sensor Placement Optimization in Modal Analysis

Joseph Morlier, Aniello Basile, Ankit Chiplunkar, M. Charlotte

An EGO-like Optimization Framework for Sensor Placement Optimization in Modal Analysis

Joseph Morlier*, Aniello Basile, Ankit Chiplunkar, Miguel Charlotte

Université de Toulouse, CNRS, ISAE-SUPAERO, Institut Clément Ader (ICA), France
*joseph.morlier@isae-supaero.fr

Abstract: In aircraft design, Ground/Flight Vibration Tests (GVT/FVT) are conducted to extract aircraft's modal parameters (natural frequencies, damping ratios and mode shapes) also known as the modal basis. The main problem in aircraft modal identification is the large number of sensors needed, which increases operational time and costs. The goal of this paper is to minimize the number of sensors by optimizing their locations in order to reconstruct a truncated modal basis of *N* mode shapes with a high level of accuracy in the reconstruction. There are several methods to solve Sensors Placement Optimization (SPO) problems, but for this case an original approach has been established based on an iterative process for mode shapes reconstruction through an adaptive Kriging Metamodeling approach so-called EGO-SPO. The main idea in this publication is to solve an optimization problem where the sensors locations are variables and the objective function is defined by maximizing the trace of criteria so-called AutoMAC. The results on a 2D wing demonstrate a reduction of sensors by 30% using our EGO-SPO strategy.

1. Introduction

Experimental Modal Analysis (EMA) is a common experimental methodology to estimate the dynamic characteristics of a structure. The identification process consists of estimating the modal parameters from a set of Frequency Response Functions (FRF). *Sensor Placement Optimization* (SPO) is a common problem encountered in many engineering applications, that has led to the development of several techniques [1,2,3]. The SPO techniques have been applied to various mechanical, aerospace, and structural systems for designing the best sensing locations, which are used to estimate modal parameters based on vibration responses [4,5].

Vibration tests on large structures such as aircrafts are however a costly and time consuming work. Typically, in aircraft design this involves a set of 500 accelerometers that, in addition to the difficulty to place them where it is appropriate, also add masses and may modify significantly then the real dynamic characteristics of the structure. In particular, the position of these vibration sensors influences the modal identification quality of structures, which for a given number of sensors is usually estimated in terms of correlation between the natural modes using the *Modal Assurance Criterion* (MAC) [7].

In the past, several works have already tried to tackle the SPO problem by various methods. Thus, Jung *et al* [8] have recently proposed a discrete-type optimization problem using Genetic Algorithm (GA). This latter was formulated by defining the sensor positions and the MAC as the design variables and the objective function, respectively. Schulze *et al* [9] have also introduced a GA approach but with a weighted off-diagonal criterion. For wind turbine identification, this approach notably yields the sensor configuration with the highest quality. Tong *et al* [10] have presented an improved simulated annealing (SA) algorithm to solve the sensor placement problem. The proposed method has been tested on a numerical slab model that consists of two hundred sensor location candidates using three types of objective functions: the determinant of the *Fisher Information Matrix* (FIM), the MAC and the *Mean Square Error* (MSE) of mode shapes. It may also be worth mentioning that optimal sensor placement is also a current trend in *Structural Health Monitoring* (SHM). *Yi et al*. has developed innovative algorithms for optimizing system sensor arrays in civil engineering [11, 12].

Besides the foregoing approaches, we have discussed in our previous work [13] of the metamodeling capability of Kriging for mode shapes reconstruction. As a different application, this paper aims now at extending our original approach to the SPO aims. Recently a global optimization strategy so called *Efficient Global Optimization* (EGO) has been developed using the *Kriging's variance information* [16] and its (improved) use is here of interest as an alternative to the previous approaches. In short, Kriging or Gaussian Process regression is a method of interpolation for which the interpolated values are modeled by a Gaussian Process governed by a prior covariance [15]. More recently it has been extended on bridge structures using an improved version of kriging, called *robust kriging* (RK) [14]. The basic idea of kriging is to predict the value of a function at a given point by computing a weighted average of the known values of the function in the neighborhood of the point.

The aforementioned EGO method becomes popular as it is an adaptive sequential method that balances local and global search, i.e. balance exploitation of some metamodels and exploration of the design space [17]. These metamodels, or surrogate models (also called experts) are notably mathematical functions tuned for approximating a black-box functions. An enhanced version of EGO was first introduced in the pioneering work of Forrester and Jones [18] where they succeed in optimizing the geometry of a passive vibration isolating truss. Besides, the machine learning community has generalized Kriging's theory into a versatile computational framework called GPML [19]. This methodology is well known in machine learning/engineering optimization for reaching a *global optimum at a fixed budget* even at in a high dimensional constrained optimization problem [20]. It also has been validated in aerodynamic shape optimization [21,22] using a modified EGO algorithm based on Mixture of Experts (MOE).
Regarding the present work, we derive *the fixed budget approach*, normally used to limit costly computer experiments, to a sensor placement optimization problem. More precisely, we want to automate the sensor placement methodology using an adaptive strategy derived from EGO for mode shapes reconstruction (a basis of *N* modes). Starting from few sensor locations (initial design of experiments), the method iteratively adds new sensors at positions that tend to maximize the function *trace(MAC)*. MAC is widely used for comparing mode shapes which is normally computed between the selected mode shapes and targeted mode shapes. In a supervised approach the targeted modes can be an analytical or FEM based. In an unsupervised methodology, the *AUTOMAC* can be used [7]. An equivalent objective function is to minimize *norm(MAC – I),* where *I* is the identity matrix. The EGO approach consists in using an analytical criterion, so-called *Expected Improvement,* to minimize/maximize an objective function.

The paper will be divided into three main parts. We first introduce theoretical background for modal analysis and metamodeling. Then the EGO-SPO original strategy will be presented step by step. A supervised test case will permit to validate EGO-SPO in 1D. Finally, two test cases based on aircraft wings will be introduced: the first one in 1D, the second one in 2D to reveal the ability of Kriging based method for mode shapes reconstruction.

2. Theoretical background

2.1. From EMA to mode shape estimation

The equations of motion for a vibrating structure are commonly derived by applying Newton's second law:

$$M\ddot{x}(t) + C\dot{x}(t) + Kx(t) = f(t) \qquad (1)$$

The excitation forces *f(t)* and responses *x(t)* are functions of time *(t)* while *M, C, K* are the mass, damping and stiffness constants respectively. The equivalent frequency domain form of the dynamic model of equation in (1) can be represented in terms of transfer function $H(j\omega)$ as:

$$H(j\omega) = \frac{X(j\omega)}{F(j\omega)} = \frac{1}{(M(j\omega)^2 + C(j\omega) + K)} \qquad (2)$$

Modal parameter estimation is a special case of system identification where the *a priori* model of the system is known to be in the form of modal parameters. The identification process considers a set of *Frequency Response Functions* (FRF) as input. Identification of the FRF by means of spectral analysis is usually considered well-investigated. A unified matrix frequency-based approach can be found for instance in [23].
We must precise however here that this paper is not dealing with errors of FRF estimation (H1, H2 etc…) [24] and so with the choice of optimal FRF estimator. The current approach in modal identification involves using numerical techniques to separate the contributions of individual modes of vibration in measurements such as FRF. Each term of the FRF matrix in Equation (2) can be represented in terms of pole location and a mode shape:

$$H(j\omega) = \frac{r_k}{(j\omega - \lambda_k)} + \frac{r_k^*}{(j\omega - \lambda_k^*)} \qquad (3)$$

In Equation (3), r_k is the (n by n) shape for the k^{th} mode (* designates complex conjugates); λ_k is the pole value for mode k = $-\zeta_k\omega_k + j\omega_k\sqrt{1-\zeta_k^2}$ where, ω_k = undamped natural frequency and ζ_k = damping ratio of mode k.

Given that this work is dedicated to find the optimal spatial sensor locations while focusing only mode shapes reconstruction techniques, one major hypothesis for this aim is that the mechanical system under study must be linear. Then the only inputs for our methodology are the estimated mode shapes (also call modal vectors, or again eigen-vectors) that could be stored in a modal basis (or again a set of eigen-vectors associated to eigen-values). Practically, it can be viewed as the response of displacement sensors giving the out-of-plane information at a certain frequency for a unitary amplitude excitation. The MAC is calculated as the normalized scalar product of the two sets of vectors $\{\phi_A\}$ and $\{\phi_B\}$. The resulting scalars are arranged into the MAC matrix:

$$MAC(r,q) = \frac{\left|\{\varphi_A\}_r^T\{\varphi_B\}_q\right|^2}{\left(\{\varphi_A\}_r^T\{\varphi_A\}_r\right)\left(\{\varphi_B\}_q^T\{\varphi_B\}_q\right)} \qquad (4)$$

In Equation (4), the matrix component *MAC(r,q)* is computed between mode *r* of the first family and mode *q* of the second family. *MAC* values oscillate between 0 and 1, the unitary value meaning a perfect correlation. In practice, a value greater to 0.9 is commonly recognized as acceptable to establish the correspondence between two mode shapes. The symbols *A* and *B* represent the two sets of mode shapes which usually refer respectively to simulation (analytical or FEA) and experimental data; the MAC matrix gives so quantitatively a good idea of the closeness between two families of mode shapes.

Stubbs and Park [25] have extended the *Whittaker–Nyquist–Kotelnikov–Shannon* sampling theorem to spatial data for avoiding the well-known problem called "aliasing". In figure 1, we can see that 9-grid points measurement are not enough precise to reconstruct the (3,1) mode shape. This example illustrates the importance of sensor placement when the natural modes of flexible structure are extracted by experiment using a limited number of vibration sensors.

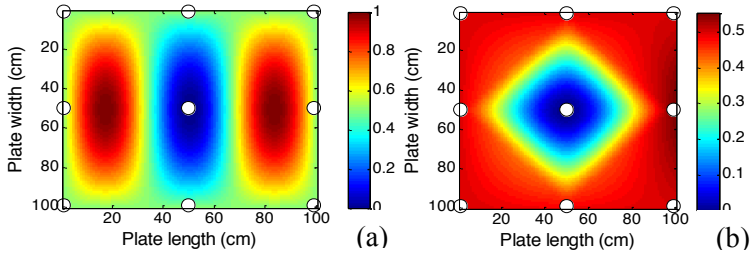

Figure 1 : (3,1) mode of vibrating plate plus regular grid distribution of sensors in white circles (a) and The cubic interpolation which shows a spatial aliasing in mode shape reconstruction (b). A regular grid of 9 sensors (white circles) permits only to reconstruct the (1,1).

In this case, there are insufficient measured degrees-of-freedom in order to discriminate between the different modes. The only solution is to measure more degree-of-freedom. However, the *MAC* can tell us whether there are enough measurement points. This is done using a version of the *MAC* called the *AutoMAC* in which a set of modes are correlated with themselves.

2.2. Metamodeling for mode shapes reconstruction

In this paper, we will concentrate in particular on some approaches which are demonstrated to be very successful at finding global solutions of black-box global unconstrained optimization problems. The main idea behind these methods is to iteratively construct metamodels to approximate the black-box functions (globally) and use them to search for optimal solutions. Complementary reviews can be found in [26,27]. A common algorithm for metamodel-based methods is as follows:

Phase 1 (design): Let k := 0. Select and evaluate a set x_0 of starting points.
While stopping criteria are not met:

Phase 2 (model): From the data {(x,f(x)) |x ∈ Sk}),
construct a metamodel mk(.) that approximates the black-box function

Phase 3 (search): Use mk(.) to search for a new point x to evaluate.
Evaluate the new chosen point, update the data set Sk. Assign k := k + 1.

Algorithm 1. Surrogate based optimization

Phase 1 is commonly referred to as sampling (also called *design of experiments*, DOE) [28]. Its purpose is to find a set of points uniformly spread over the domain, so that, if we evaluate the function at these points, we might obtain a global representation of its range. Latin Hypercube Sampling (LHS) is the most popular method to perform sampling [29].

In Phase 2, various models can be used to approximate black-box functions. In the next section, we will introduce some of the most popular models, including polynomials, *radial basis functions* (RBF) and kriging.

Phase 3 is the crucial step in this common algorithm. Given the information from the current metamodel, we need to choose which point(s) should be evaluated in the subsequent step (so called enriching point). The most common strategy is to select the next point for evaluation as the one that maximizes (or minimizes) the merit function (also known as cost function).

2.3. Definition of the chosen metamodeling techniques

In this section, we choose to introduce the chosen metamodeling techniques and explain them using in few basic steps. Three models will be studied here: Polynomial Approximation (PA), Radial Basis Function (RBF) and Kriging.

A polynomial approximation of $\hat{f}$ of order *m* can be written, in the one-variable case, as:

$$\hat{f}(x, m, w) = \sum_{i=0}^{m} w_i x^i \qquad (5)$$

We want to estimate the weight vector $w = \{w_0, \ldots, w_m\}^T$ in Equation (5) through the solution of $y = \Phi w$, where Φ is the *Vandermonde's* matrix. The maximum likelihood estimate of *w* is $w = \Phi^+ y$, where $\Phi^+ = (\Phi^T \Phi)^{-1} \Phi^T$ is the *Moore-Penrose* pseudo-inverse matrix. This gives an estimation of *w* at chosen order *m.* Obviously, the problem can be extended to more variables, while considering this general equation:

$$\hat{f}(x) = \sum_{i=1}^{n_b} w_i \psi^{(i)} \qquad (6)$$

In Equation (6), the ψ are picked from a basis truncated at order *m*. For example, with $m = 2$, $\psi^{(i)} \in \{1, x_1, x_2, x_1x_2, x_1^2, x_2^2\}$.

As an alternative, a more interesting metamodel can be used. The radial basis function approximation is given by:

$$\hat{f}(x) = w^T \psi = \sum_{i=1}^{n_c} w_i \psi\left(\left\|x - c^{(i)}\right\|\right) \qquad (7)$$

In Equation (7), $c^{(i)}$ denotes the i^{th} of the n_c basis function centers and ψ is the n_c -vector containing the values of the basis functions ψ evaluated at the Euclidean distances between the prediction site *x* and the centers $c^{(i)}$ of the basis functions. The classical basis function used is the cubic one $\psi(r) = r^3$. Whether we choose a set of parametric basis functions or fixed ones, *w* is easy to estimate, via interpolation condition. Albeit the equation is linear in terms of the basis function weights w, yet the predictor $\hat{f}$ can express highly nonlinear responses. It is easy to see that one of the conditions of obtaining a unique solution is that the system must be square, that is $n_c = n$. Simplifications arise if the bases actually coincide with the data points, that is $c^{(i)} = x^{(i)}$, which leads to the equation $\Psi w = y$, where Ψ is the *Gram* matrix, defined as $\Psi_{i,j} = \psi\left(\left\|x^{(i)} - x^{(j)}\right\|\right)$ for $i,j = 1, \ldots, n$. The fundamental

step of the parameter estimation process is to calculate $w = \Psi^{-1} y$. Of course, the choice of the basis functions can have important effects on the metamodel prediction [17].

Finally, we will present a more versatile metamodel so called *Kriging*. Originally developed for geostatistic purposes, Kriging is a method of interpolation for which the interpolated values are modeled by a Gaussian process governed by prior covariances [15]. It assumes that the spatial variation of an attribute is neither totally random, nor deterministic. Today, it is widely used in other domain of engineering and often called Gaussian Process Regression (GPR). This method uses a linear combination of all sampling values, their weights determined by their distances from the interpolation point. This requires therefore some knowledge about the relation between the distance and the covariance to be described. The Kriging method is merely built by injecting a basis function in Equation (7) defined as:

$$\psi^{(i)} = exp\left(-\sum_{j=1}^{k} \theta_j \left|x_j^{(i)} - x_j\right|^{p_j}\right) \qquad (8)$$

In equation (8), the vector θ allows to vary the width of the basis function from variable to variable. This equation (8) is also known as *Standard Exponential* (SE) kernel. Interested reader can find the detailed procedure used in [17]. The exponent *p* can vary for each dimension in x. We denote this by using a set of random vectors $Y = \{Y(x_1), \ldots, Y(x_n)\}^T$. The random variables are correlated with each other with the *Kriging* basis function $\psi^{(i)}$, from which it's possible to construct the correlation matrix Ψ and the covariance matrix $cov(Y,Y)=\sigma^2\Psi$ of size *n*. This assumed correlation between the sample data reflects our expectation that an engineering function will behave in a certain way. The correlations depend on the absolute distance between the sample points and on the parameters *p* and *θ*. For example, with a very low value of *p* there is no immediate correlation between the points. The parameter *θ* is a width parameter that affects how far a sample point's influence extends. A low *θ* means that there is high correlation between points; a high *θ* means the contrary. We can also consider *θ* as a measure of how 'active' is the function that we are approximating. The main problem is then to choose *p* and *θ*. A solution can be maximizing the likelihood of *y* using classical optimizer (gradient based, genetic algorithms etc…) [16-19].

We can then compute the prediction and so-called *predict* function using the Forrester's toolbox [17]:

$$\hat{y}(x) = \hat{\mu} + \varphi^T \psi^{-1}(y - I\hat{\mu}) \qquad (9)$$

The parameter $\hat{\mu}$ (mean) can be defined as:

$$\hat{\mu} = \frac{I^T \psi^{-1} y}{I^T \psi^{-1} I} \qquad (10)$$

The associated variance s^2 as:

$$s^2(x) = \sigma^2\left(1 - \varphi^T \psi^{-1} \varphi \quad + \frac{(1 - I^T \psi^{-1} \varphi)2}{I^T \psi^{-1} I}\right) \qquad (11)$$

where $\sigma^2 = \frac{(y - I\hat{\mu})^T \psi^{-1} (y - I\hat{\mu})}{n}$.

2.4. Illustrative example on a clamped plate (supervised case)

Let us precise our problem of mode shapes reconstruction. The design space belong to R^3 and can be defined as *(x,y,Z)*. Here (*x,y)* represents the sensor location, and Z is the local mode shape value. The goal is to learn from this database of examples the true mode shape basis. Thus, the estimation of mode shapes reconstruction accuracy will increase together with the sampling density. Of course, the complexity will grow when taking into account triaxial sensors but this is not in the scope of this paper. The performance of our algorithm is defined by the number of evaluations needed (so called *fixed budget*) until an acceptable (global) solution is found. One stopping criterion can be the maximum number of sensors. The objective is to optimize the locations of sensors for the purpose of making the most accurate predictions of the mode shapes at unmeasured locations. We use a MATLAB based *Finite Element model* (FEM) of a plate, an eigenvalue solver for modal analysis. The presented test case is a clamped plate. The Fixed-Free plate has one clamped edge and three free ones (CFFF). It has been done to build a supervised data. Thus, we can compute standard prediction criteria such as *Root Mean*

Square Error (RMSE). This is a frequently used measure of the differences between values predicted by a model or an estimator $\hat{y}$ and the values actually observed *y*. The RMSE expresses the average model prediction error in units of the variable of interest. It is calculated as:

$$RMSE = \sqrt{\frac{1}{n}\sum_{j=1}^{n}\left(y_j - \hat{y}_j\right)^2} \qquad (12)$$

The used geometrical and material properties are: *length=width= 0.8m, height= 0.01m, E = 210e9 Pa, nu = 0.33, rho = 7700*. A dedicated mesh is used to obtain the truncated reduced basis $\{\Phi_1, \Phi_2, .., \Phi_N\}$. In practice we use the nine first bending modes from mode (1,1) to mode (3, 3). Each classical reconstruction method has been compared with these supervised data. Three types of sampling have been used (regular grid, random grid, and pseudo random grid). Appendix A illustrates the result for a regular grid of 24 sensors with the mode (3,3). The pseudo-random grid is made for a half part with uniformly spaced sensors while sensors are added randomly for the other half part. Table 1 resumes the results of the presented metamodeling techniques (averaged 10 times).

CFFF PLATE		REGULAR GRID		RANDOM GRID		PSEUDO RANDOM GRID	
		Average Max RMSE	Average Mean RMSE	Average Max RMSE	Average Mean RMSE	Average Max RMSE	Average Mean RMSE
METHOD	RSM cubic	1,4624	0,4024	3,0812	0,7632	34,3243	6,9853
	RBF cubic	0,2091	0,0741	0,1731	0,1026	0,4333	0,1364
	Kriging (from [15])	0,2051	0,0699	0,1500	0,0707	0,2449	0,0963
	Kriging (ordinary)	0,3757	0,1520	0,3341	0,2007	0,4450	0,2026

Table 2. Summary of RMSE for each reconstruction method for the entire modal basis (9 first bending modes of the CFFF plate). Kriging from [17] exhibits the lowest RMSE from all the selected methodology.

This preliminary study confirms that Kriging is very well adapted to the mode shape reconstruction problem because it gives in each case the lowest RMSE.

3. Sensor Placement Optimization inspired from Efficient Global Optimization

3.1. EGO

As already mentioned, the EGO algorithm [16] is an adaptive optimization method based on kriging. An initial design of experiment is used to build a first metamodel. In the present study, the MATLAB function, lhsdesign, was used to obtain the LHS points with the default criterion (maximin). This criterion maximizes the minimal distance between points: it proceeds by iteratively generating a number of LHS samples at random and chooses the best one based on the criterion maximin. To generate the experimental design (sample), the number of sample points is specified. A new point that maximizes a criterion is chosen as optimizer candidate at each iteration. The criterion uses a tradeoff between the metamodel value and the conditional variance. Then the new point is evaluated using the original model and the metamodel is re-learnt on the extended design of experiment. The original criteria use the Kriging variance information to maximize the Expected Improvement (so called *EI*). The EGO algorithm tends to explore the design space while trying to exploit the region with the global optimum. Given equations 6 and 7, EI is given by:

$$E[I(x)] = \begin{cases} \left(y_{min} - \hat{y}(x)\right)\Phi\left(\frac{y_{min}-\hat{y}(x)}{\hat{s}(x)}\right) + s\varphi\left(\frac{y_{min}-\hat{y}(x)}{\hat{s}(x)}\right) & if\ s > 0 \\ 0 & if\ s = 0 \end{cases} \qquad (13)$$

Here $\Phi(.)$ and $\varphi(.)$ are the cumulative distribution function and probability density function respectively. In many situations maximizing $E[I(\mathrm{x})]$ will prove to be the best way to finding the global optimum [16]. In the equation (10) it is possible to see two terms separated by '+'. The first one is the exploitation term and is based more on the improvement at *x*, while the second one is the exploration term and is based more on the amount of the error. As advocated by the literature, one of the strong points of EGO is the balance between exploration and exploitation. But one can give more importance to one of these terms (depending on the problem), simply by adding a "weight" (Hybrid Criteria in [16]). In particular, sometimes the EI can present very strong peak. Sassena *et al* [30] proposed a smoother criterion so-called WB2 often preferred to EI.

3.2 EGO like Strategy: EGO-SPO

In this section, we explain our strategy by introducing how the sensor placement optimization problem for modal basis reconstruction (involving *N* modes) is solved step-by-step. It can be seen using Equation (4) that the orthogonality between the modal bases increases as the off-diagonal values decrease to zero while the diagonal terms approach to unity. That is, the modal identification of flexible structure by experiment becomes more accurate as the sensor placement produces the *MAC* closer to the above-mentioned ideal one.
Here, the *MAC* is always a function of *x*, the sensor set locations. In the general (unsupervised) case, we only have a set of experimental measurements X, so we use compute *AutoMAC* as:

$$AutoMAC(r,q) = \frac{\left|\{\varphi_X\}_r^T\{\varphi_X\}_q\right|^2}{(\{\varphi_X\}_r^T\{\varphi_X\}_r)(\{\varphi_X\}_q^T\{\varphi_X\}_q)} \qquad (14)$$

We will solve two equivalent unconstrained bounded optimization problems solved using EGO. The equation (15) introduces the maximization of *trace(AutoMAC)* for blind reconstruction*:*

$$\max_x \quad \left(\mathrm{trace}\left(\mathrm{AutoMAC(x)}\right)\right)$$
$$\text{with respect to } \mathrm{x} \in \mathrm{D} \qquad (15)$$

Where *x* is the sensor set locations, *D* is the geometry of the structure under study, *I* is the identity matrix of size *N*.

The following equation gives an equivalent minimization:

$$\min_x \quad \left(\mathrm{norm}\left(\mathrm{AutoMAC(x)}\right) - \mathrm{I}\right)$$
$$\text{with respect to } \mathrm{x} \in \mathrm{D} \qquad (16)$$

In the supervised example of the next paragraph, we will use standard *MAC* to compare analytical mode shapes (modal basis *A*) to reconstructed mode shapes (modal basis *B*). It will be then possible to compute RMSE and control the robustness of our methodology.

EGO-SPO strategy consists in a two steps metamodels construction (Figure 2): first we build the mode shapes Mk(.) from an initial DoE, then we compute a prediction of the objective function mk(.) according to Algorithm 1. It can be noticed that one stopping criterion can also be a maximal number of sensor (at fixed budget). Both objective functions have been tested and the results are very close for each test case.

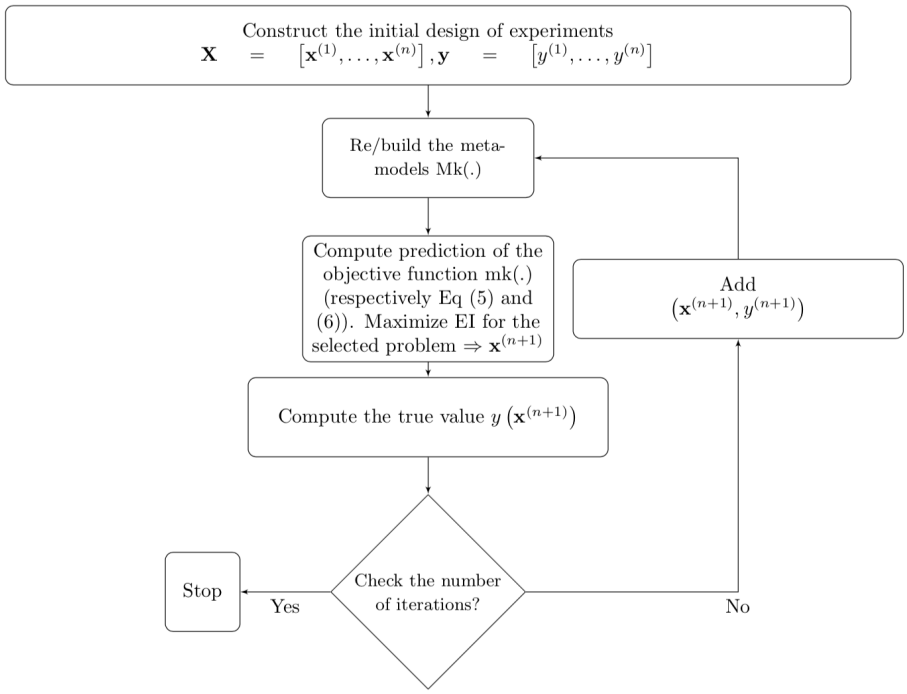

Figure 2. Steps used for the EGO-SPO strategy

3.3 Supervised Case with analytical data: Cantilever Beam

We use in this paragraph a supervised approach in order to compare the results of our reconstruction methodology to analytical results. In this case since we have the analytical solution *AutoMAC* is not needed. The mode shapes of a cantilever beam are given by the analytical formula:

$$\varphi_n(x) = A_n\left(cosh\, m_n x - cos\, m_n x - \left(\frac{sinh\, m_n L - sin\, m_n L}{cosh\, m_n L + cos\, m_n L}\right)(sinh\, m_n x - sin\, m_n x)\right) \quad (17)$$

Here A_n is a constant (It can be used to normalize the mode shape), $m_n = (2n-1)\pi/2L$, L is the length of the beam and n is the number of the mode.

Figure 3 shows the iterations that will lead to add a new sensor. The figure 3b shows the construction of the function “prediction of *trace(MAC)”,* in which only five initial points have been used. Then, evaluating the EI at each iteration (each reconstruction) a new point is added, where EI is maximal, and the function is updated (figure 3a). The new sensor will be located where the “prediction of *trace(MAC)”* is maximal (figure 3b).

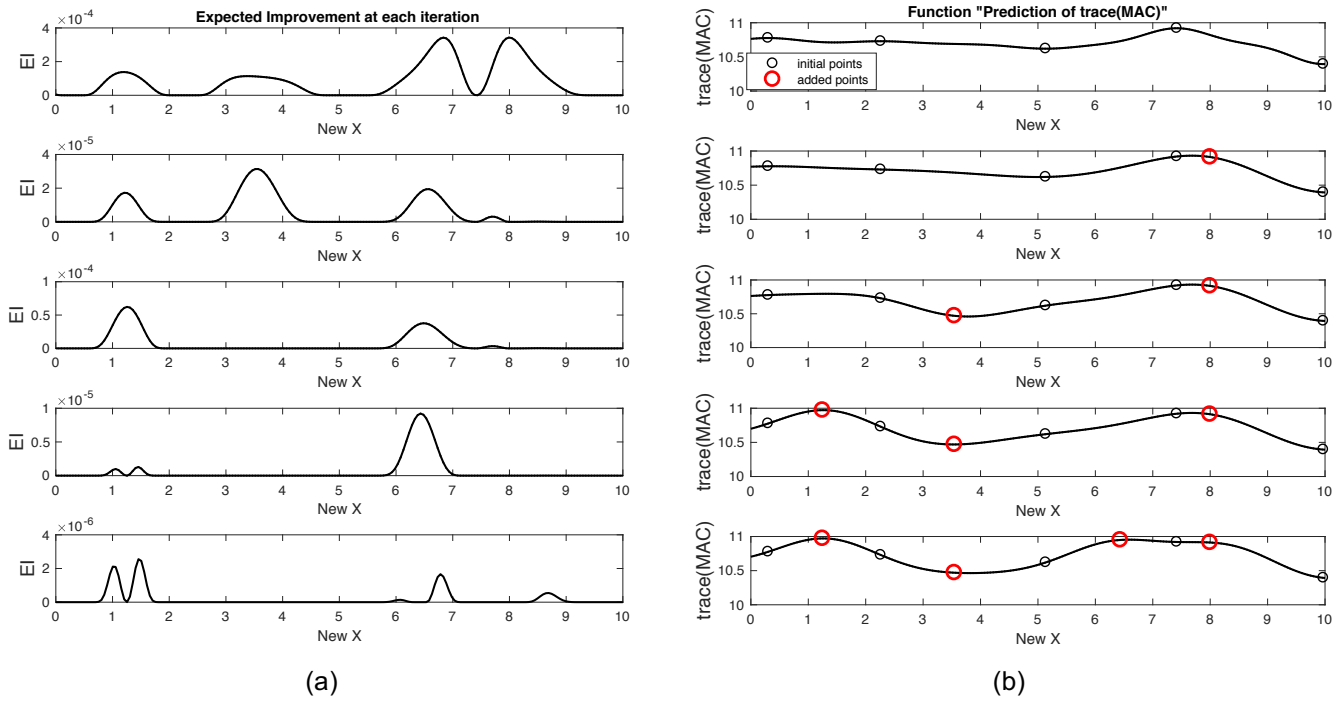

Figure 3. Inside the strategy. On the left, the EI that determines the updating. On the right, the updating of prediction of trace(MAC).

In the figure 4, convergence of the objective function is shown for three different LHS initial DOE. All the sensors (maximum budget) have been added and *trace(MAC)* is maximized (equal to N, the modal basis size).

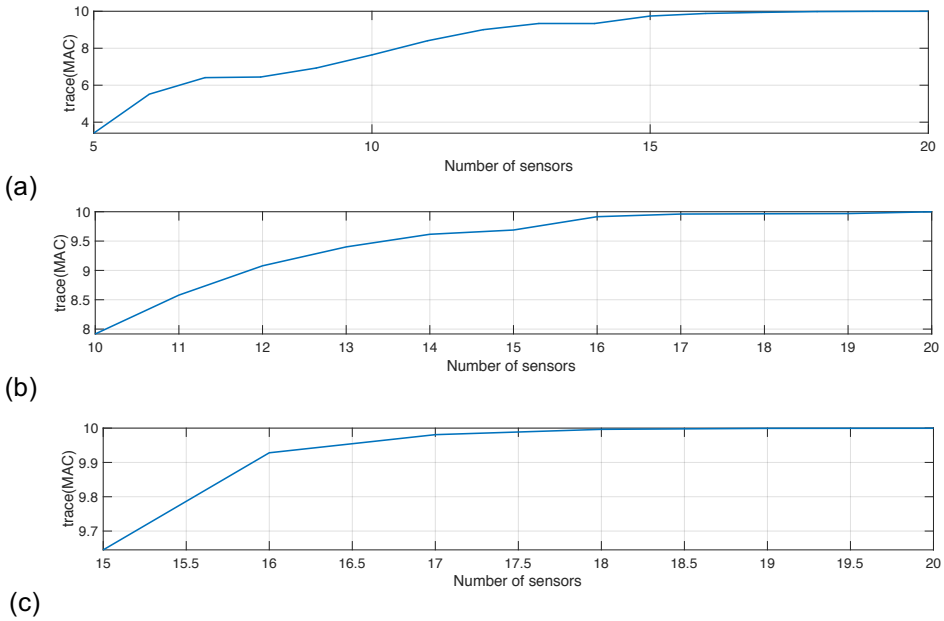

Figure 4. Convergence of objective function maximization (to 10) with a maximum number of 20 sensors (a) Initial DOE: LHS with 5 points. (b) Initial DOE: LHS with 10 points. (c). Initial DOE: LHS with 15 points

Since we are in supervised approach we can compute the RMSE. For all constructed metamodels they achieve the fixed tolerance (*1E-3*) while *trace(MAC)* is maximized after 20,18 and 16 iterations respectively for initial DOE of 5,10,15 respectively. It becomes clear from Figure 4 that the final reconstruction is DOE-dependent. With the larger initial DOE, the RMSE is lower for each reconstruction and the convergence of the objective function is faster. These conclusions are important for the next chapter.

4. Blind reconstruction: Results and discussion

4.1 1D wing: Embraer EMB 120 Brasilia

In this paragraph, we analyze a 1D Wing but with operational constraints (fuel cells and engine mass are notably considered). To extract the modal data, we used a MATLAB toolbox compatible with NASTRAN inputs called CoFE [31]. CoFE is an open-source program for structural analysis and design. It supports linear statics, vibration eigenpair (eigenvalues and eigenvectors), and buckling eigenpair analysis. Since the code uses NASTRAN formatted input, commercial preprocessing tools (e.g. PATRAN) it can be used to create or check the bulk data inputs. The mode shapes have here been normalized.
We choose to analyze only bending modes around the Z axis (Figure 5). The studied wing is a cantilever beam with three concentrated masses that represent the engine and two fuel cells of the Embraer EMB 120 Brasilia from [32]. It can be found schematically in the following figure:

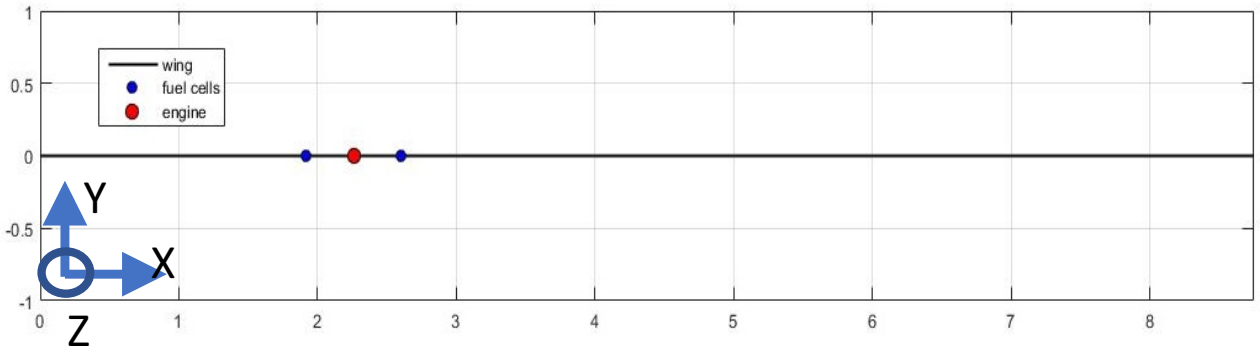

Figure 5. Schematization of the Wing, with Engine and fuel cells length (8m).

We used a test case with a modal basis of size *N*=12 with maximum 30 sensors. The *AutoMAC* is used instead of MAC for blind reconstruction using *trace(MAC)* as an objective function. On figure 6, we can see that the convergence is fast: only 7 additional sensors are needed (no need to reach the maximum budget).

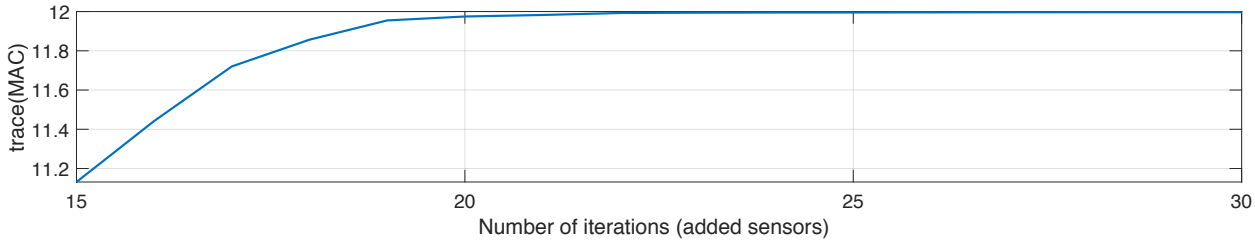

Figure 6. Convergence of the objective function *trace(MAC)*, from mode 1 to 12. Initial DOE: LHS with 15 points. Max number of sensors: 30.

Figure 7 shows only qualitatively the Kriging reconstruction, obtained using an initial LHS design of experiment and adding 7 points optimizing the objective function *trace(MAC)* through the EGO-SPO strategy, is quite good. Using this approach, we are optimizing the placement of the sensors for all the desired mode-shapes at once.

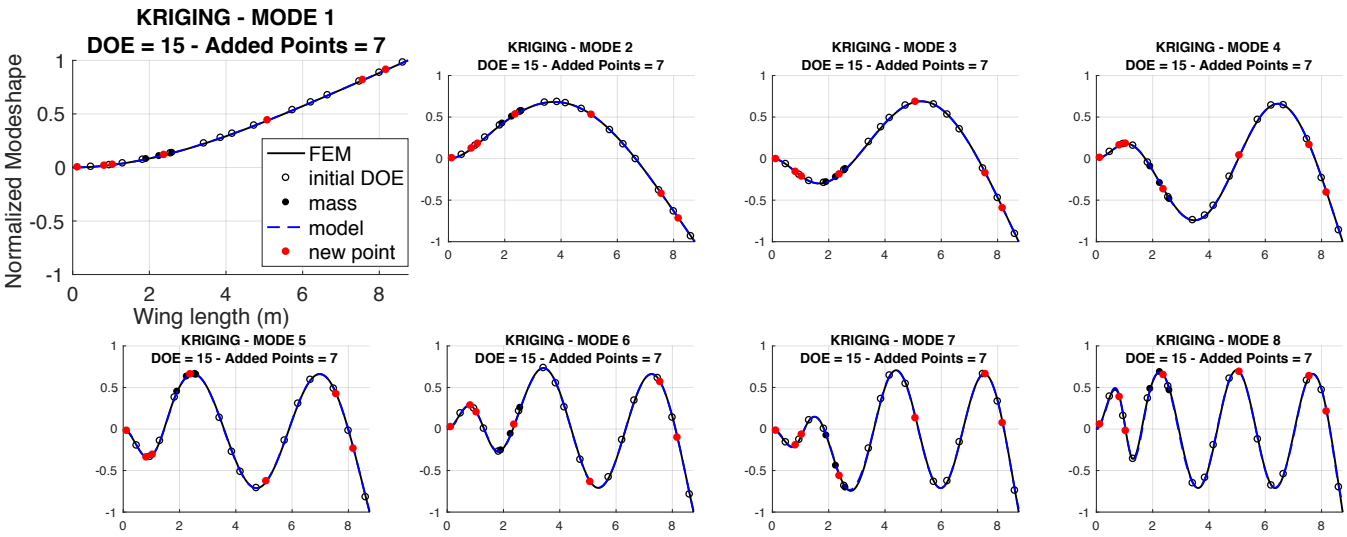

Figure 7. Reconstruction of mode shapes, from 1 to 8. Initial DOE: LHS with 15 points. Added sensors: 7.

Qualitatively, it is also relevant to underline the difference between a Kriging and a linear reconstruction of mode shapes. Figure 8 shows this difference, where the total number of points is 25, distributed in a regular grid for the linear reconstruction, while for the Kriging reconstruction they have been placed with the EGO-SPO strategy.

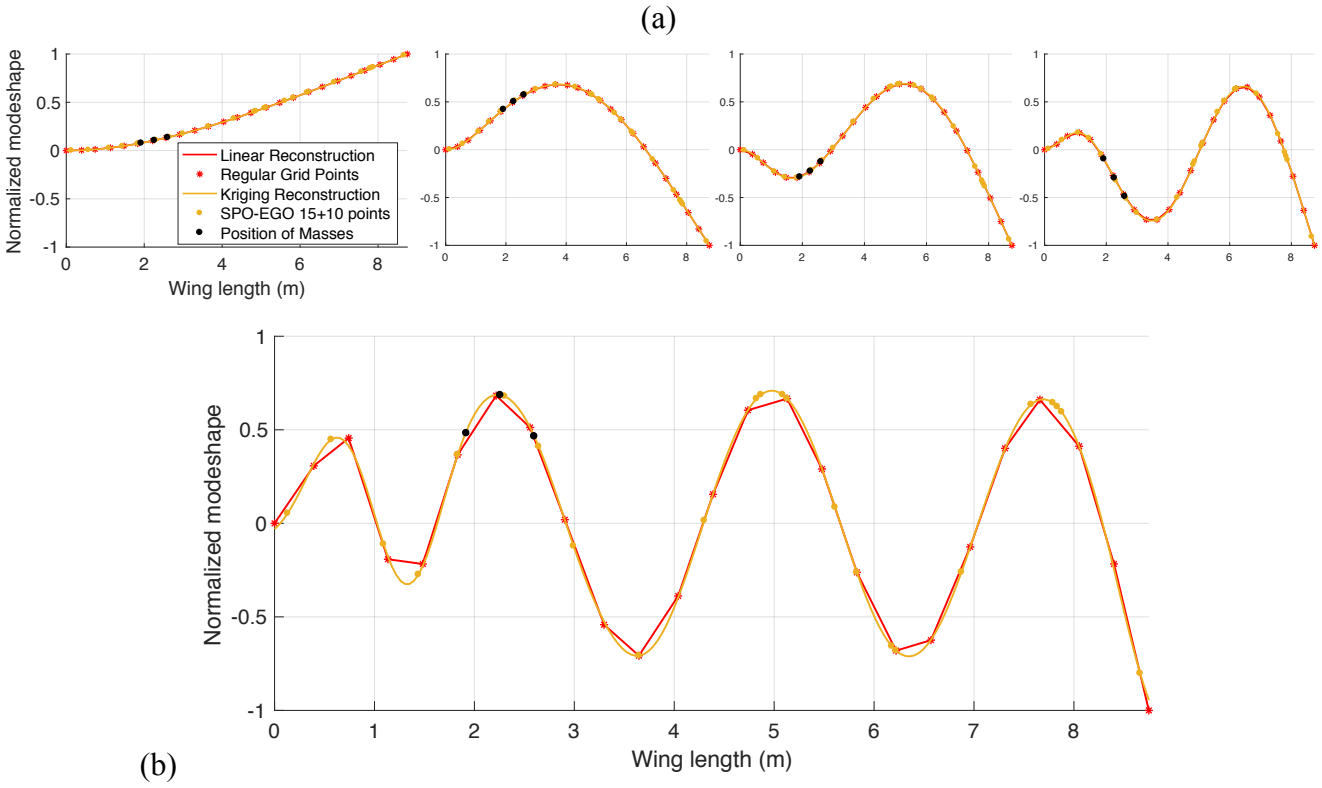

Figure 8. Comparison between Linear Reconstruction and Kriging. (a) first 4 modes, (b) zoom on mode 8 to clearly see the difference between classical linear interpolation and Kriging reconstruction

In this case the EGO-SPO strategy is capable of good reconstruction even at high frequency (mode 8 on figure 8b) with few sensors needed (22) compared to standard strategy such as linear reconstruction and Kriging (figure 8a)

4.2 2D Wing (Trapezoidal)

In order to demonstrate EGO-SPO gains on a more realistic example, we choose to analyze a 2D Wing using the MATLAB COFE. The wingspan is 4m length. We use Al_2024-T3 materials. The total number of nodes in the FE model is approximately 600 to ensure convergence on the highest natural frequency (9th mode). The mode shapes have been normalized hereafter. We aim at reconstructing the modal basis (N=9) with at most 25 sensors. The *AutoMAC* is used instead of *MAC* for blind reconstruction. In this example, we choose to minimize norm(MAC – I) starting from an initial DOE of size 15 (Figure 9). The previous supervised test cases help us to tune our strategy.

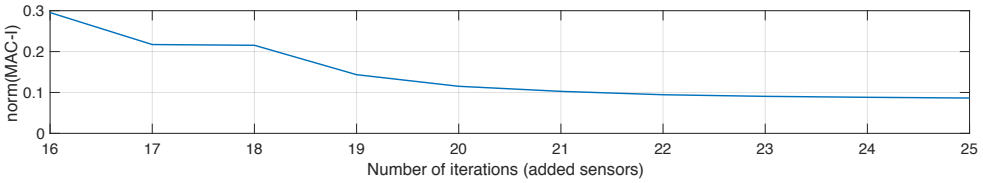

Figure 9. Convergence of the objective function *norm(MAC – I)*, from mode 1 to 9. Initial DOE: Regular Grid with 15 points. Maximum number of sensors: 25.

The figure 10 shows the performance of EGO-SPO strategy, comparing reconstructions of 9th mode shape of the wing. Each reconstruction is compared to the High-Fidelity model (HF) that practically comes from FEM data and is shown on the left wing. Kriging reconstruction without the optimization strategy needs 36 sensors (regular grid) to reach a good level of reconstruction, compared to HF data, while the linear reconstruction with 36 sensors does not give a good result. This sensor placement strategy allows a reduction of 30.56% of sensors for the entire modal basis with only 25 sensors (15 initial regular DOE + 10 added sensors). The results of the EGO-SPO strategy is illustrated on the figure 14 in Appendix B. The complexity here, is closed from an industrial test case as the chosen modal basis exhibits bending modes, torsion modes, plus some coupling modes (bending & torsion).

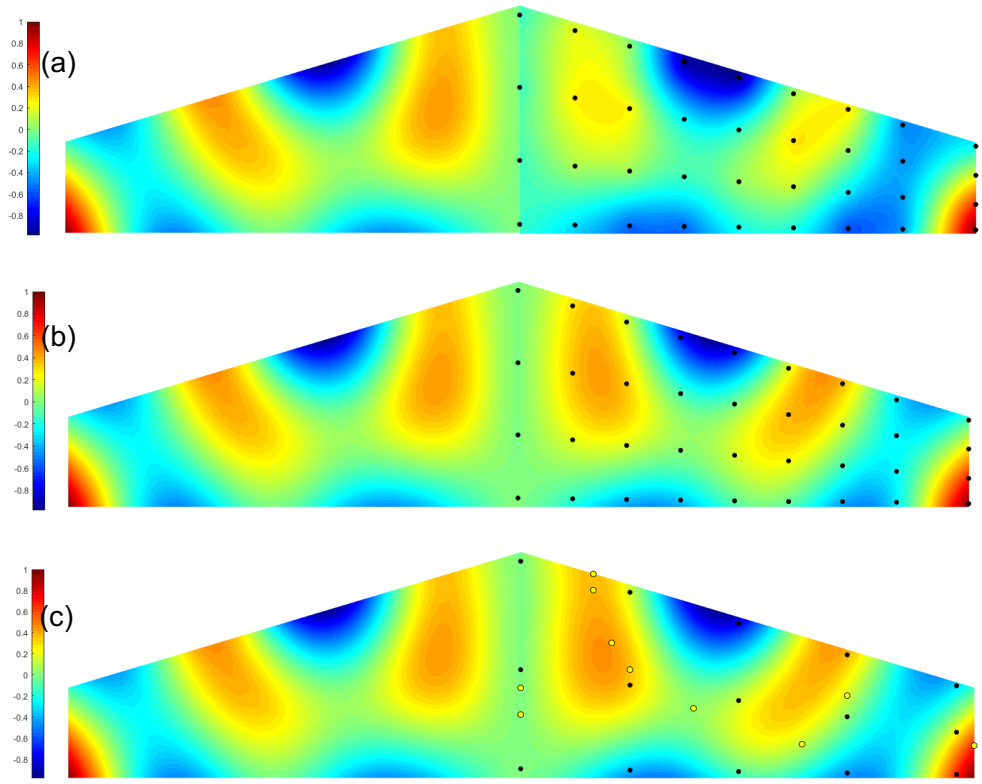

Figure 10. (a) Comparison between HF FEA results (left) and a Linear Reconstruction with a regular grid of 36 sensors (right), for 9th Mode Shape. (b) Comparison between HF FEA results (left) and a Kriging Reconstruction with a regular grid of 36 sensors (right), for 9th Mode Shape. (c) Comparison between HF FEA results (left) and EGO-SPO strategy (right) The black dots represent the initial DOE (regular grid, 15 sensors). The yellow ones represent 10 added sensors. This sensor placement strategy allows a reduction of 30.56% of sensors for the entire modal basis.

Conclusion

In this paper, we developed a new strategy so called EGO-SPO dedicated to modal analysis based on an *adaptive Kriging Metamodeling* approach. The quality of modal identification is classically estimated using the *MAC* (or *AutoMAC*) criterion. We first proposed a totally supervised numerical experiments in order to calibrate the methodology. Then we proposed some “blind” modal basis reconstruction on 1D and 2D wing structures. The performance of the reconstruction outperforms existing methodology (linear reconstruction, RBF, ordinary Kriging). The gain is almost 30% less sensor for the same level of reconstruction on the trapezoidal example. The developed MATLAB software can be used both for benchmarking (supervised mode), sensor placement strategy using FEM (calibration) or experimental data (FVT, GVT). Of course, this methodology is sensitive to the initial DOE, we propose to work at fixed sensors budget will help the vibration engineer to make the best choice for his experimental test rig. Our future work will be dedicated to aeroelastic calibration of a full aircraft. Co-Kriging will be used to build a model with two kinds of data. For example, it will permit to merge lots of low fidelity FE model denoted as cheap data with few expensive data (experimental data or high fidelity models) in the same metamodel.

Acknowledgements

The authors really want to thank Claire Meyer from Dassault aviation for given us industrial inputs and Nathalie Bartoli from ONERA for her advice on the developed methodology.

References

[1] Kammer, D. C. (1991). Sensor placement for on-orbit modal identification and correlation of large space structures. Journal of Guidance, Control, and Dynamics, 14(2), 251-259.

[2] Minwoo C. and S. N. Pakzad, Optimal Sensor Placement for Modal Identification of Bridge Systems Considering Number of Sensing Nodes, Journal of Bridge Engineering, 2014.

[3] Minwoo C.and S. N. Pakzad, Optimal sensor configuration for flexible structures with multi-dimensional mode shapes, Smart Materials and Structures, 2015.

[4] Yuan, C., & Zhang, J. (2014, October). An approach to optimal sensor placement for vibration tests on large structures. In Internoise and noise Congress, Conference Proceedings (Vol. 249, No. 7, pp. 1111-1116).

[5] Ewins D.J., Modal Testing: Theory, Practice and Applications, 1984.

[6] Avitabile P., Experimental Modal Analysis – A Simple Non-Mathematical Overview, Sound & Vibration, 2001.

[7] Allemang, R. J. (2003). The modal assurance criterion–twenty years of use and abuse. Sound and vibration, 37(8), 14-23.

[8] Jung, B. K., Cho, J. R., & Jeong, W. B. (2015). Sensor placement optimization for structural modal identification of flexible structures using genetic algorithm. Journal of Mechanical Science and Technology, 29(7), 2775-2783.

[9] Schulze, A., Zierath, J., Rosenow, S. E., Bockhahn, R., Rachholz, R., & Woernle, C. (2016, September). Optimal sensor placement for modal testing on wind turbines. In Journal of Physics: Conference Series (Vol. 753, No. 7, p. 072031). IOP Publishing.

[10] Tong, K. H., Bakhary, N., Kueh, A. B. H., & Yassin, A. Y. (2014). Optimal sensor placement for mode shapes using improved simulated annealing. Smart Struct. Syst, 13(3), 389-406.

[11] Yi, T. H., Li, H. N., & Zhang, X. D. (2012). A modified monkey algorithm for optimal sensor placement in structural health monitoring. *Smart Materials and Structures*, *21*(10), 105033.

[12] Yi, T. H., Li, H. N., & Gu, M. (2011). Optimal sensor placement for structural health monitoring based on multiple optimization strategies. *The Structural Design of Tall and Special Buildings*, *20*(7), 881-900.

[13] Morlier, J., Chermain, B., & Gourinat, Y. (2009). Original statistical approach for the reliability in modal parameters estimation. In MAC XXVII a conference and exposition on structural dynamics, Orlando, USA.

[14] Simon, P., Goldack, A., & Narasimhan, S. (2016). Mode shape expansion for lively pedestrian bridges through Kriging. Journal of Bridge Engineering, 21(6), 04016015.

[15] Matheron G., Principles of Geostatistics, Economic Geology, 58, 1246-1268, 1963.

[16] Jones, D. R., Schonlau, M., & Welch, W. J. (1998). Efficient global optimization of expensive black-box functions. Journal of Global optimization, 13(4), 455-492.

[17] Forrester, A., & Keane, A. (2008). Engineering design via surrogate modelling: a practical guide. John Wiley & Sons.

[18] Forrester, A., & Jones, D. (2008) Global optimization of deceptive functions with sparse sampling. In 12th AIAA/ISSMO multidisciplinary analysis and optimization conference, Victoria, British Columbia, Canada.

[19] Rasmussen, C. E., & Williams, C. K. (2006). Gaussian Processes for machine learning (Vol. 1). Cambridge: MIT press.

[20] Bouhlel, M., Bartoli, N., Regis, R. G., Otsmane, A., & Morlier, J. (2018). Efficient global optimization for high-dimensional constrained problems by using the Kriging models combined with the partial least squares method. Engineering Optimization, 1-16.

[21] Bartoli, N., Bouhlel, M. A., Kurek, I., Lafage, R., Lefebvre, T., Morlier, J., ... & Regis, R. (2016). Improvement of efficient global optimization with application to aircraft wing design. In *17th AIAA/ISSMO Multidisciplinary Analysis and Optimization Conference* (p. 4001).

[22] Bartoli, N., Lefebvre, T., Dubreuil, S., Olivanti, R., Bons, N., Martins, J., ... & Morlier, J. (2017). An adaptive optimization strategy based on mixture of experts for wing aerodynamic design optimization. In *18th AIAA/ISSMO Multidisciplinary Analysis and Optimization Conference* (p. 4433).

[23] Allemang, R. J., & Brown, D. L. (1998). A unified matrix polynomial approach to modal identification. Journal of Sound and Vibration, 211(3), 301-322.

[24] Shin, K., & Hammond, J. (2008). Fundamentals of signal processing for sound and vibration engineers. John Wiley & Sons.

[25] Stubbs N., Park, S., and Sikorski Optimal sensor placement for mode shapes via Shannon's sampling theorem. Microcomputers in civil engineering, 11, 411-419, 1996.

[26] Vu, K. K., D'Ambrosio, C., Hamadi, Y., & Liberti, L. (2017). Surrogate-based methods for black-box optimization. International Transactions in Operational Research, 24(3), 393-424.

[27] Queipo, N. V., Haftka, R. T., Shyy, W., Goel, T., Vaidyanathan, R., & Tucker, P. K. (2005). Surrogate-based analysis and optimization. Progress in aerospace sciences, 41(1), 1-28.

[28] Sacks, J., Welch, W. J., Mitchell, T. J., & Wynn, H. P. (1989). Design and analysis of computer experiments. Statistical science, 409-423.

[29] Morris, M. D., & Mitchell, T. J. (1995). Exploratory designs for computational experiments. Journal of statistical planning and inference, 43(3), 381-402.

[30] Sasena M. J., Papalambros P. Y., Goovaerts P., Metamodeling Sampling Criteria in a Global Optimization Framework, Symposium on Multidisciplinary Analysis and Optimization, 2000.

[31] Ricciardi, A. P., Canfield, R. A., Patil, M. P., and Lindsley, N., Nonlinear Aeroelastic Scaled-Model Design, Journal of Aircraft, Vol. 53, No. 1 (2016), pp. 20-32.

[32] Venkataraman, P. Blending Classical and Practical Instruction in Structural Mechanics Using COMSOL, Proceedings of the COMSOL Users Conference Boston, 2007.

Appendix A

The figures 11, 12 and 13 illustrate the CFFF plate. This is supervised example, RMSE and R^2 can be computed using a true (converged mesh) finite element model. The coefficient of determination, denoted R^2. It provides a measure of how well observed outcomes are replicated by the model, based on the proportion of total variation of outcomes explained by the model. R^2 can be calculated as:

$$R^2 = \frac{SS_{reg}}{SS_T} = 1 - \frac{SS_{res}}{SS_T} = 1 - \frac{\sum_{i=1}^{n}(y_i - f_i)^2}{\sum_{i=1}^{n}(y_i - \bar{y})^2}.$$

Here SS_{reg} is the regression sum of squares, SS_{res} is the residual sum of squares, SS_T is the total sum of squares. R^2 is a measure of how much of the variance in y is explained by the model, f.

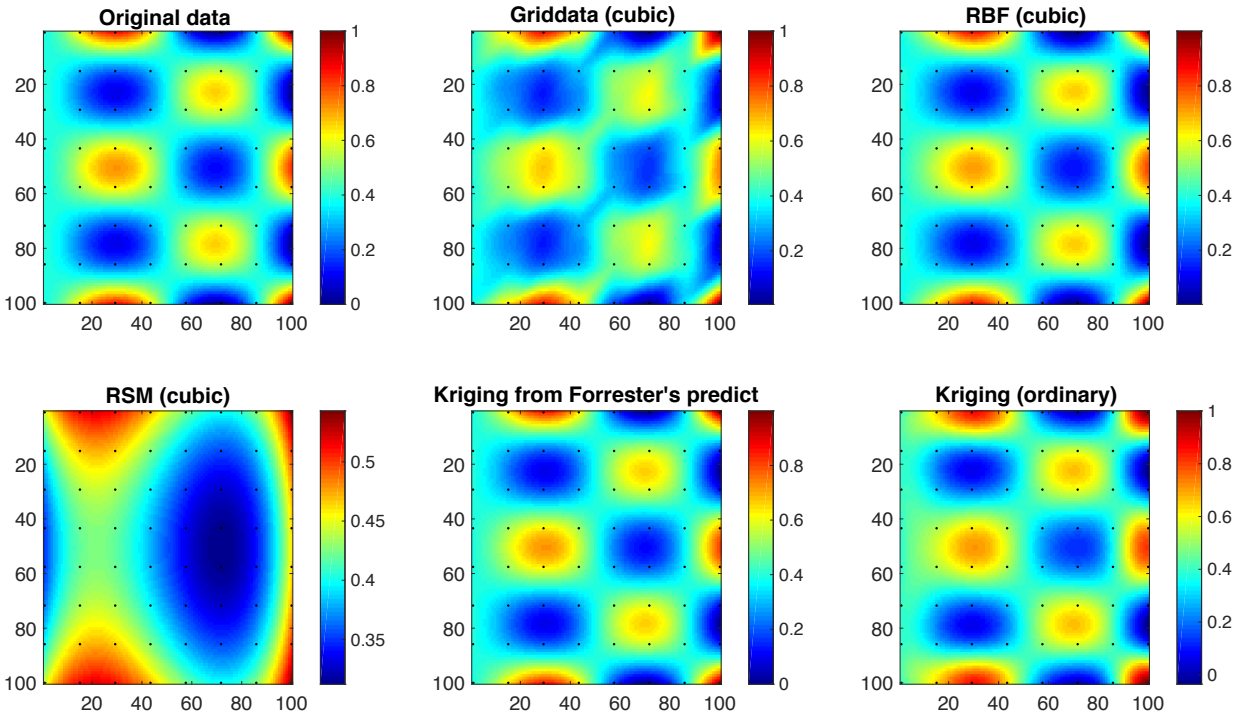

Figure 11. Reconstruction of Mode Shape (3, 3) of a CFFF plate, with a regular grid of 64 sensors (final grid). RSM cubic reconstruction demonstrates the aliasing problem

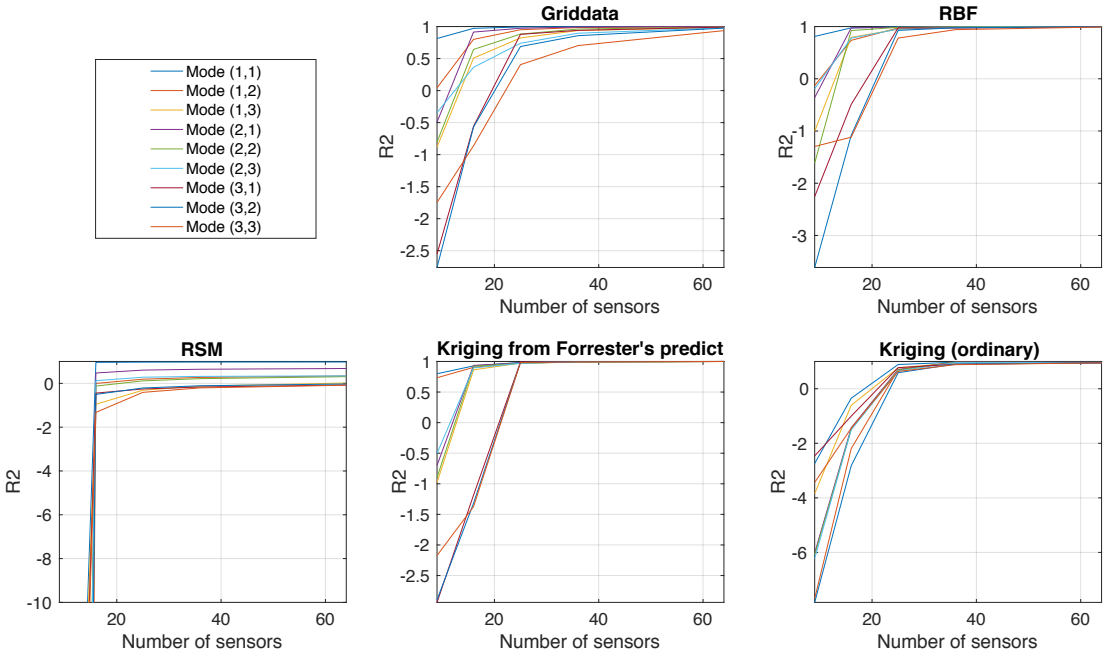

Figure 12. R^2 for increasing number of Sensors, from mode (1, 1) to (3, 3), regular grid, CFFF plate.

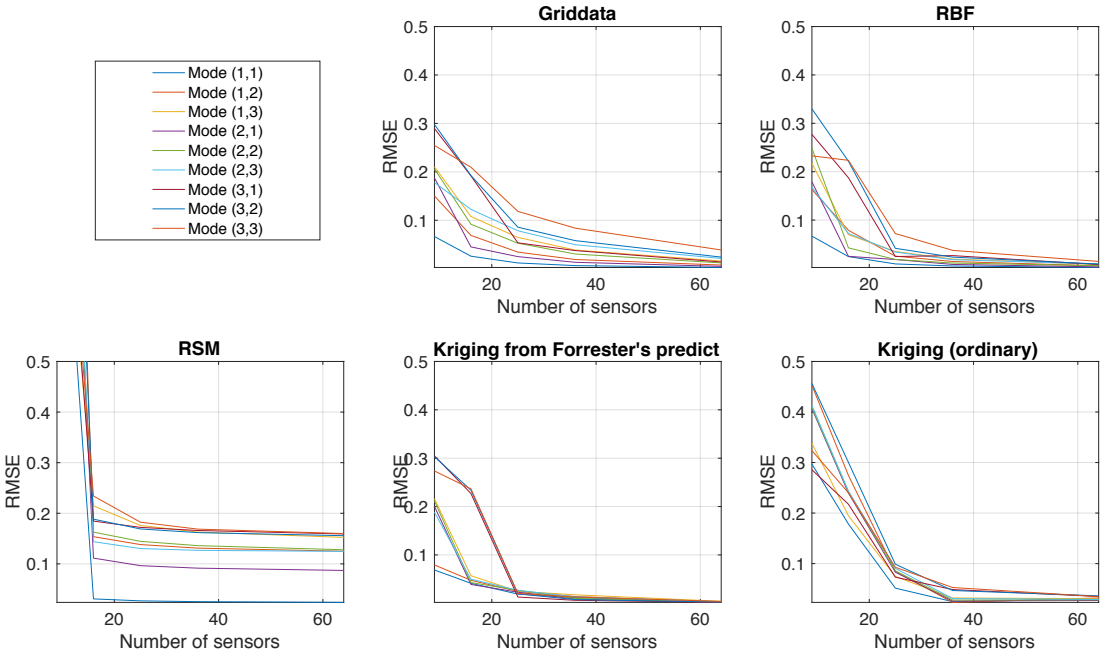

Figure 13. RMSE for increasing number of Sensors, from mode (1, 1) to (3, 3), regular grid, CFFF plate.

Appendix B

As an example, the reconstruction of 9 first bending modes of the 2D trapezoidal wing has been inserted in the figure 14. The chosen modal basis exhibits bending, torsion, plus some coupling mode (bending and torsion).

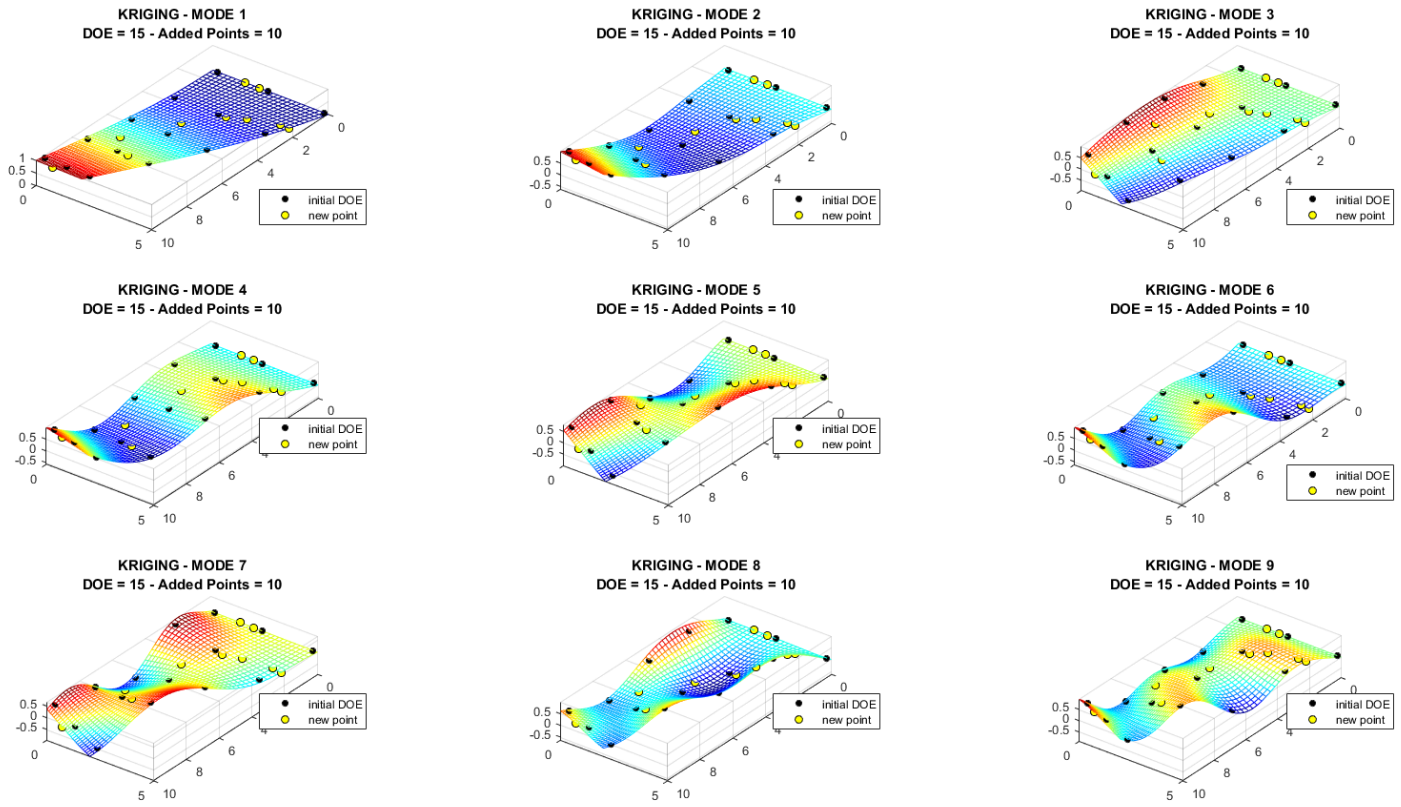

Figure 14. Reconstruction of mode shapes, from 1 to 9. Initial DOE: Regular grid with 15 points. Maximal number of sensors: 25. The initial DOE is represented by black dot, the new point chosen by EGO-SPO strategy in yellow.